Journal of Materials Chemistry B

ROYAL SOCIETY OF CHEMISTRY

PAPER

View Article Online
View Journal | View Issue

Cite this: J. Mater. Chem. B, 2023, 11, 5494

A thermo-responsive hydrogel loaded with an ionic liquid microemulsion for transdermal delivery of methotrexate†

Yang Shu, [a] Rong Xue,[b] Yiru Gao,[c] Wenxin Zhang[c] and Jianhua Wang *[c]

Systemic administration of methotrexate (MTX), the gold standard for the treatment of psoriasis, can cause adverse side effects. To address this issue, a thermally responsive hydrogel loaded with an ionic liquid microemulsion (IL-ME) was developed for the transdermal delivery of MTX. The microemulsion was prepared using water, Tween 20 and choline and geranic acid (CAGE) ionic liquid. The solubility of methotrexate in the IL-ME was 9-fold higher than that in phosphate buffer (PBS). The hydrogel (Gel) based on isopropylacrylamide and silk fibroin acts as a drug reservoir to achieve temperature-responsive drug release in the human epidermis. The loading of the IL-ME or MTX-containing IL-ME on the Gel produced a ME@Gel or MTX/ME@Gel. *In vitro* permeation experiments showed that the MTX/ME@Gel exhibited a 27.6% increase in MTX permeation. In addition, IL-ME exhibits strong antibacterial activity. *In vivo* studies indicated that when compared with the results obtained in PBS medium, the MTX/ME@Gel could effectively treat skin redness, swelling and scaling caused by imiquimod (IMQ). In general, the present study demonstrated that the MTX/ME@Gel provides vast potential to serve as a biocompatible drug carrier for the efficient delivery of poorly soluble drugs, *i.e.*, MTX in this particular case.

Received 13th October 2022,
Accepted 13th November 2022

DOI: 10.1039/d2tb02189g

rsc.li/materials-b

10th Anniversary Statement

The authors' group has had very tight relations with the *Journal of Materials Chemistry B* since its first launch in 2013. It has provided a very good forum for us for the dissemination and discussion of our research and innovations in the field of materials sciences dedicated to biology and medicine. The main research interests of our group have been focused on the design of special structures for interaction with proteins and for their isolation & analysis, the development of drug carrier systems for therapeutic applications, and the exploration of novel platforms for bio-sensing & cellular imaging purposes. We have published 23 articles in this journal in the period of 2013–2021 (with one most cited), with a total citation of *ca.* 900. In the future, further studies will still be focused on the above issues. At its 10th Anniversary, we sincerely hope that the *Journal of Materials Chemistry B* will further develop its honourable reputation in the related fields of materials sciences.

1. Introduction

Psoriasis is a chronic autoimmune disorder manifested as auto-amplification and hyper-proliferation of the epidermis, affecting more than 100 million people worldwide.[1–5] Generally, the gold standard drug for the treatment of psoriasis, *i.e.*, methotrexate (MTX), is an immunosuppressive modulator that inhibits the activity of proliferating keratinocytes.[6–10] In practice, however, MTX has low solubility, poor permeability and low bioavailability.[11,12] Topical drug delivery avoids the hepatic first-pass effects commonly encountered with oral medications, which may improve bioavailability and prevent drug degradation, and thus avoid some undesirable side effects.[13–15] In this respect, the Transdermal Delivery Drug System (TDDS) has received widespread attention in the field of pharmaceutical technology. However, the stratum corneum (SC) greatly weakens the efficacy of the drug due to the difficulty of penetrating the skin barrier.[16] Thus, in the last few decades, studies have focused on the exploration of effective technical means to break through the skin barrier and promote the penetration rate of drugs.[17–23]

It is known that ionic liquids (ILs) consist of organic cations and organic/inorganic anions and they exhibit unique

[a] *Northeastern University School of Materials Science and Engineering, Shenyang, China*
[b] *Northeastern University, Department of Chemistry, Shenyang, China*
[c] *Northeastern University, Research Center for Analytical Sciences, Shenyang, China. E-mail: jianhuajrz@mail.neu.edu.cn*

† Electronic supplementary information (ESI) available. See DOI: https://doi.org/10.1039/d2tb02189g

physicochemical properties. Recent studies have found that ILs composed of choline cations and organic acid anions are nontoxic, highly biocompatible and biodegradable, which meet the standards of medical chemical penetration enhancers.[24–27] In addition, ILs can promote the transdermal delivery of small-molecule drugs, even some macromolecules, proteins, and RNAs. Choline and geranic acid (CAGE) have been used as penetration enhancers for the transdermal delivery of insulin and siRNA.[28–38] A microemulsion (ME) is a thermodynamically stable isotropic transparent solution consisting of at least hydrophilic, hydrophobic and amphiphilic components. The microemulsion constructed by ILs, termed IL-ME, may combine the advantages of both ILs and ME, *i.e.*, high solubility, strong permeability, favorable thermal stability, tunable structures and properties, and facile preparation.[39–45] Choline fatty acid IL-ME has been demonstrated to improve the solubility and permeability of a variety of poorly soluble drugs, *e.g.*, celecoxib, acyclovir, methotrexate, and dantrolene sodium.[13,39,46,47]

Hydrogels can act as drug reservoirs for sustainable drug release.[48,49] The drugs in the gel act directly on the wound through physical contact, with little involvement in blood circulation, which greatly reduces the toxicity and side effects caused by systemic administration. The structure of hydrogels may change in response to physical and chemical stimuli in the environment, *e.g.*, temperature,[50] pH,[51,52] and enzymes.[53] Poly(*N*-isopropylacrylamide) (PNIPAM) hydrogels are widely used to develop thermally responsive drug delivery systems due to their lower critical solution temperature (LCST).[54] At a temperature above the LCST (32 °C), PNIPAM transforms from a hydrophilic state to a hydrophobic state. In this process the hydrogel network shrinks and expels the drug from the gel. However, the poor mechanical properties and the easy rupture of pure PNIPAM hydrogels limit its application in tissue engineering.[55] Silk fibroin from *Bombyx mori* has been widely used as a biomaterial for decades due to its multiple advantages, *e.g.*, good biocompatibility, controllable degradability, and favorable mechanical properties.[56] Therefore, silk fibroin provides a useful candidate for the construction of hydrogel networks, which endows PNIPAM with good mechanical properties.

Herein, we report a thermally responsive hydrogel based on an ionic liquid microemulsion (IL-ME) for the transdermal delivery of methotrexate. The IL-ME was constructed using CAGE together with Tween 20. Silk fibroin (SF) and isopropylacrylamide (NIPAM) co-constructed a physicochemical double-crosslinked hydrogel (Gel), which not only maintained the thermally responsive properties, but also enhanced the mechanical properties and adhesion capability (Scheme 1). MTX exhibits favorable solubility in the IL-ME wherein the permeability of MTX is significantly enhanced. *In vitro* studies illustrated that the present thermally responsive hydrogel has antibacterial properties and low cytotoxicity. Further experiments with mice demonstrated its capability in the transdermal delivery of MTX, which effectively treated imiquimod-induced skin inflammation with no adverse side effects.

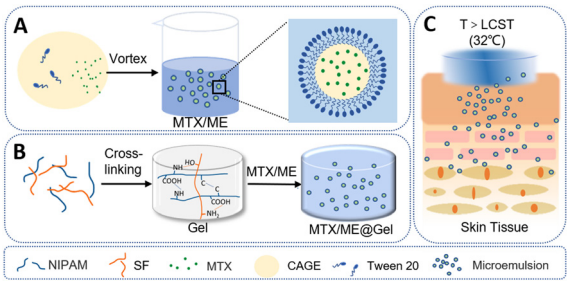

Scheme 1 Schematic diagram for the preparation of the MTX/ME@Gel and its drug release process. (A) Preparation of IL-ME. (B) Preparation of Gel and MTX/ME@Gel. (C) The response of the drug release on the skin.

2. Experimental

2.1 Materials

Choline hydroxide, geranic acid, *N*-isopropylacrylamide, isopropyl myristate (IPM) and polyethylene glycol (PEG) were provided by Shanghai Macklin Biochemical Co (Shanghai, China). *N*,*N*-Dimethylformamide (DMF) and ethyl acetate (EA) were obtained from Tianjin Fuyu Fine Chemical Co (Tianjin, China). Ammonium persulfate (APS) and dimethyl sulfoxide (DMSO) were provided by the Tianjin Damao Chemical Reagent Factory (Tianjin, China). *N*,*N*′-Methylenebisacrylamide (MBA), methotrexate hydrate (MTX), benzaldehyde (BzH), *N*,*N*,*N*′,*N*′-tetramethylethylenediamine (TEMED), silk fibroin (SF) and Tween 20 were acquired from Aladdin Industrial Co (Shanghai, China). Hoechst 33,342 and propidium iodide (PI) were the products of YEASEN (Shanghai, China). 3-(4,5-Dimethylthiazol-2-yl)-2,5-diphenyltetrazolium bromide (MTT) was supplied by KeyGEN BioTECH (Nanjing, China). Hematoxylin–eosin (H&E) stain was bought from Biosharp Life Sciences (Anhui, China). Luria–Bertani (LB) agar and Trypticase Soy Broth (TSB) were received from Beijing Aoboxing Bio-tech Co. Ltd. RPMI-1640 medium was bought from Thermo Scientific. All the reagents were used without further purification.

Female 5-week-old (BALB/6) mice weighing 18–20 g were supplied by Huafukang China, Inc. The mice were housed at 25 ± 2 °C in an environment with 60 ± 10% relative humidity and were subjected to a natural light/dark cycle for at least 1 week prior to the tests. They were handled and controlled in accordance with the guidelines provided by the Animal Ethics Committee of Northeastern University, China.

2.2 Preparation and characterization of an IL-ME

Geranic acid and choline were mixed in a molar ratio of 2 : 1 and stirred at room temperature for 48 h until the solution became sticky. The mixture was then kept in a vacuum concentrator for 6 h to remove majority of water molecules followed by drying for 24 h to obtain ionic liquid choline and geranic acid (CAGE). The prepared CAGE was then mixed with Tween 20 and water in a volume ratio of 1 : 1 : 3 and stirred at room temperature for 3 h to obtain the IL-ME. MTX was dissolved in the IL-ME to obtain a MTX-containing

microemulsion termed MTX/ME (with MTX concentrations of 1, 10, 15 and 17.5 mg mL^{-1}).

The particle sizes of the IL-ME and MTX/ME were obtained by transmission electron microscopy (TEM) and dynamic light scattering (DLS) at room temperature. The IL-ME or MTX/ME was passed through a 0.22 μm filter to remove insoluble impurities. For TEM imaging, the IL-ME or MTX/ME was dropped on an ultra-thin carbon membrane. The excessive solvent was removed with filter paper after allowing it to stand for 5 min. A drop of 2% phosphotungstic acid was then used to cover the IL-ME or MTX/ME and allowed to stand for 5 min for negative staining. After completely drying, TEM images were obtained at an accelerating voltage of 120 kV. For DLS analysis, the IL-ME or MTX/ME with various concentrations of MTX (1, 10, 15, and 17.5 mg mL^{-1}) was taken into a glass cell for measurements.

The stability of microemulsion systems was evaluated by observing the particle size variations of the IL-ME and MTX/ME at 4, 25 and 37 °C. The fresh IL-ME was allowed to stand at room temperature for 30 days, and the particle size was measured on days 1, 5, 10, 20, and 30.

2.3 Preparation of the hydrogel and IL-ME loaded hydrogel and their properties

The hydrogel was prepared using the following procedure. 0.1 g mL^{-1} *N*-isopropylacrylamide, 0.1 g mL^{-1} silk fibroin, 0.1 g mL^{-1} crosslinker MBA, and 0.1 g mL^{-1} initiator APS were mixed in a sample vial with a volume ratio of 1 : 0.2 : 0.005 : 0.005. 3 μL of TEMED was then added and the mixture was allowed to stand for 5 min to react completely. The sample vial was placed in a water bath at 40 °C until the hydrogel had shrunk uniformly, which was collected and rinsed with deionized water to remove the unreacted monomers. After lyophilization, the hydrogel was immersed in 2 mL of IL-ME or MTX/ME and fully expanded to obtain a microemulsion loaded ME@Gel or MTX/ME@Gel.

The tensile strength of the Gel was assessed using an Instron Tensile Tester (SANS, CMT6502, USA). The Gel was cut into a strip with a thickness of 2 mm and a length of 20 mm. The measurement was conducted at a tension speed of 10 mm min^{-1}. The various parameters, *i.e.*, elastic modulus, elongation at break, tensile stress at break, tensile strength and maximum tensile force, were recorded.

The swelling ratio was also measured. The Gel with different concentrations of SF was freeze dried to obtain its dry weight (m_0). It was then immersed in 10 ml IL-ME or PBS (10 mM, pH 7.4). The weight of the swollen hydrogel (m_t) was measured every 30 min until complete saturation (3 replicates). The swelling ratio was calculated using the following equation:

$$\text{Swelling ratio (\%)} = (m_t - m_0)/m_0 \times 100$$

The spreadability of the Gel with different concentrations of SF (0, 0.05, 0.1, 0.15, and 0.2 w/w) was evaluated at 21 °C ± 0.5 °C after 48 h of preparation. Each Gel (diameter of 10 mm) was placed on a round glass plate (diameter of 9 cm) and covered with the same plate. A weight of 500 g was placed on the upper glass plate and left for 24 h at room temperature, and the spreading diameter was measured (3 replicates).

The occlusivity of the PBS@Gel, ME@Gel and fluocinonide cream was evaluated by an *in vitro* occlusion test. 250 mL beakers were filled with 200 mL of distilled water, covered with filter paper (cellulose acetate filter, 90 mm) and carefully sealed with tape. Each gel or fluocinonide cream was uniformly spread evenly on the surface. The samples were kept at 32 °C (skin temperature) for 48 h in an incubator. A control was prepared similarly without the Gel. The weights of the samples were taken after 24 h or 48 h to determine water loss due to evaporation.

The occlusion factor (F) was calculated as in the following (3 replicates), with A as the water loss without the Gel (control) and B as the water loss with the Gel or fluocinonide cream.

$$F = (A - B)/A \times 100.$$

2.4 The maximum solubility of drugs in various solvents

The excessive amount of MTX was added into 1 mL of phosphate buffer solution (PBS), IL-ME, *N*,*N*-dimethylformamide (DMF), dimethyl sulfoxide (DMSO), ethyl acetate (EA), isopropyl myristate (IPM), and polyethylene glycol (PEG), respectively. The undissolved MTX was filtered out using a membrane with 0.22 μm pores. The absorbance of the filtrate at 302 nm was measured, and the maximum solubility of MTX in different solvents was derived.

2.5 Skin permeation studies

The thermally responsive drug release behavior and transdermal capability of the hydrogels were investigated. A semipermeable membrane (2000 kDa) was cut in the middle and fixed on the Franz diffusion cell with the side for drug passage to confront the donor chamber with the drug-loaded hydrogel, *i.e.*, the MTX/ME@Gel. The receiving chamber was filled with PBS (10 mM, pH 7.4). The MTX/ME@Gel (1 mL of 1 mg mL^{-1} MTX/ME) was placed over the semipermeable membrane. The Franz diffusion cell was covered with a plastic wrap to prevent evaporation. The drug release rate at 25 °C and 37 °C were measured under vortex shaking. 0.2 mL of the solution was taken from the receiving chamber every 30 min, and an equal volume of PBS (10 mM, pH 7.4) was added to maintain a constant volume of the reaction mixture therein.

For the investigation of drug penetration, pig skin was adopted and cut into circular pieces with a radius of 20 mm and a thickness of 1.5 mm. The cuticle was fixed in the Franz diffusion cell facing the donor chamber. The donor chamber contained the drug-loaded hydrogel, and the receiving chamber was filled with PBS (10 mM, pH 7.4). The control group used PBS (10 mM, pH 7.4) as the solvent, while the experimental group used the IL-ME as the solvent. The Franz diffusion cell was covered with a plastic wrap to prevent evaporation of water. It was placed in a shaker at 37 °C for 48 h. 0.2 mL solution was removed from the receiving chamber at intervals to determine

the amount of drug permeating the skin. An equal volume of receiving solution was added to maintain a constant volume in the receiving chamber.

Absorbance at 302 nm was measured using a microplate reader (BioTek, Synergy™). The cumulative release rate and permeability of the drug in the hydrogel were calculated as in the following:[57]

$$Q_n(\%) = \left(VC_n + \sum_{i=1}^{n-1} C_i V_i \right) \Big/ A \times 100$$

with Q_n as the cumulative percentage of permeated MTX, V as the volume of the medium (10 mL), C_n and C_i as MTX concentrations in the medium at time points of n and $(n - 1)$, V_i as the volume of the medium at different time points (0.2 mL), and A as the feeding quantity of MTX.

2.6 Evaluation of antibacterial activity

S. aureus (CMCC 26003) and *E. coli* (CICC10907) were used to evaluate the antibacterial activity of the MTX/ME@Gel. Bacteria were inoculated on the LB solid medium to obtain pure single colonies. One colony was transferred to the liquid medium and incubated at 200 rpm for 6 h. The bacterial suspension (1 mL) was centrifuged and the supernatant was discarded. It was then diluted with PBS (10 mM, pH 7.4) to a concentration of 2×10^7 CFU mL^{-1}. Afterwards, PBS (100 μL), PBS@Gel (100 μL PBS), ME@Gel (50 μL ME), MTX/ME@Gel-1 (50 μL of 1 mg mL^{-1} MTX/ME), and MTX/ME@Gel-2 (100 μL of 1 mg mL^{-1} MTX/ME) were incubated with 500 μL bacteria for 30 min, respectively. The bacterial suspension (100 μL) was taken and applied on the plate, which was incubated at 37 °C for 24 h. Pictures were taken and colonies were counted. The dependence of the antibacterial activity on the dosage of the IL-ME was obtained by incubating with different volumes of IL-ME (0, 25, 50, 75, and 100 μL) for 45 min. The time-dependent antibacterial activity was obtained by incubating with 100 μL IL-ME for different times (0, 15, 30, 45, and 60 min). The bacterial suspension was fixed with 2.5% glutaraldehyde at 4 °C for 4 h, and then dehydrated with alcohol gradient. The *S. aureus* suspension (20 μL) was dropped on the carbon support film and allowed to stand until it dries. The morphology of *S. aureus* was observed by scanning electron microscopy (SEM, Hitachi, SU8000, Japan).

In order to determine the minimum inhibitory concentration, the IL-ME was taken into a 96-well plate and diluted with LB medium to various concentrations (0, 3, 6, 12, 25, 50, 100, and 200 μg mL^{-1}). The LB medium without bacteria was used as the positive control, while the medium with *S. aureus* served as the blank control. 100 μL of bacteria (2×10^7 CFU mL^{-1}) was added to each well and cultured in an incubator at 37 °C for 24 h. The absorbance at 600 nm was measured with a microplate reader, and the absorbance–concentration curve was derived to determine the minimum inhibitory concentration.

2.7 *In vitro* toxicity assessment

The human normal hepatocyte L-02 was used to evaluate the cytotoxicity of the MTX/ME@Gel. L-02 was cultured in RPMI-1640 medium. 200 μL of the cell suspension was added to a 96-well plate and incubated for 10 h at 37 °C in a 5% carbon dioxide atmosphere. After the bottom of the 96-well plate was observed to be full of cells under a microscope, the IL-ME was added to obtain the final concentrations of 0, 3, 6, 12, 25, 50, 100, and 200 μg mL^{-1}. After incubation for 24 h and 48 h, 10 μL MTT was added and further incubation for 4 h was conducted. The supernatant in the well was removed, followed by the addition of DMSO (100 μL) and shaking for 10 min to dissolve the crystals completely. The absorbance at 490 nm was recorded using a microplate reader.

2.8 *In vivo* treatment and histopathological examination

Histopathological examinations were performed to determine the skin irritation and drug permeability of the MTX/ME@Gel in female BALB/c mice according to the literature.[58] Briefly, 16 mice were divided into four groups (4 × 4). The back hair of each mouse was removed to facilitate subsequent application of ointments and hydrogels. The psoriasis model was established by continuously applying 5% imiquimod cream on the back of the mice to induce dermatitis in the first week. The four groups of mice were treated with PBS (10 mM, pH 7.4), MTX/PBS@Gel (1 mg mL^{-1} MTX, 1 mL MTX/PBS), MTX/ME@Gel (1 mg mL^{-1} MTX, 1 mL MTX/ME), and fluocinolone B6 cream on the 1st, 3rd, 5th, and 7th day. At the same time, the redness and swelling of the skin and the weight changes of mice were recorded. The mice were euthanized on the last day, and their internal organs were removed along with drug-treated skin. The internal organs were soaked in formaldehyde solution overnight, and then the heart, liver, spleen, lungs and kidneys were encapsulated with paraffin. The organs were cut into 10 μm slices followed by staining with H&E. The histopathological characteristics were observed under a microscope (Olympus BX53M, Japan).

FITC was used to study the transdermal effect of the IL-ME. The skin of psoriatic mice was treated with the FITC/PBS@Gel (1 mg mL^{-1} FITC, 1 mL FITC/PBS) and FITC/ME@Gel (1 mg mL^{-1} FITC, 1 mL FITC/ME) for 24 h. The excised skin was directly cryosectioned, and then the transdermal effect was observed under a fluorescence microscope.

3. Results and discussion

3.1 Characterization of the IL-ME and ME@Gel

Scheme 1 illustrates the preparation of the IL-ME by simply mixing Tween 20, CAGE and water. The TEM images and particle size distribution of the IL-ME in Fig. 1(A) and (C) indicated an average size of *ca.* 20 nm for the micellar particles. It is seen that the incorporation of MTX in the IL-ME led to an obvious increase in the size of the micellar particles, and the increment was positively correlated with the amount of the loaded MTX (Fig. 1(B) and (D) and Fig. S1, ESI†). This

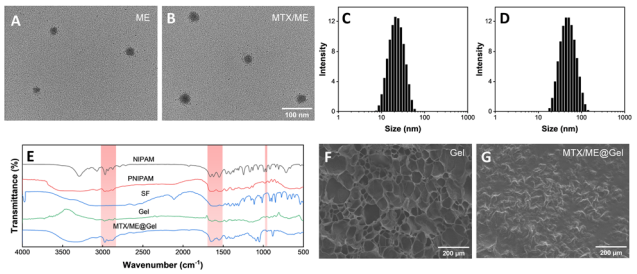

Fig. 1 TEM images of the IL-ME (A) and MTX/ME (15 mg mL^{-1}) (B) along with their size distributions in (C) and (D). FT-IR spectra of NIPAM, PNIPAM, SF, Gel, and MTX/ME@Gel (E). SEM images of the Gel (F) and MTX/ME@Gel (G).

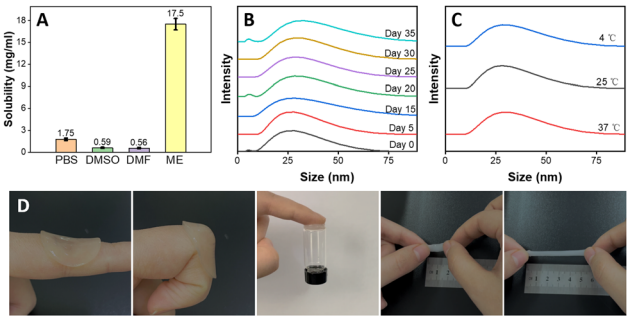

Fig. 2 (A) The significant improvement in the solubility of the MTX IL-ME. (B) Size distribution of the micellar particles in the IL-ME after standing for different times (0–35 days). (C) Size distribution of the micellar particles in the IL-ME at different temperatures (4 °C, 25 °C and 37 °C). (D) Schematic illustration of the adhesion and mechanical properties of the Gel.

observation indicated that the drug may be encapsulated in the hydrophobic core of the micelles. The surface charge analysis illustrated a zeta potential of −19.3 mV for CAGE, while it was increased to −2.66 mV after the formation of the IL-ME. This provided further evidence for the encasement of CAGE in water to form the IL/W ME (Fig. S2, ESI†). The thermally responsive gel adopted isopropylacrylamide as the backbone and silk fibroin was doped to form a physicochemical double cross-linked hydrogel. Since silk fibroin is rich in $–NH_2$ and –COOH groups, it can be connected to the backbone through hydrogen bonding, which improved the mechanical properties of the gel. The FT-IR spectrum further illustrated the formation of the Gel (Fig. 1(E)). It is obvious that the NIPAM monomer exhibited an absorption at 979 cm^{-1} corresponding to C=C. The disappearance of this band in the FT-IR spectrum of PNIPAM is due to polymerization during the formation of the hydrogel. The SF monomer has characteristic absorptions of amide I and amide II at 1650 cm^{-1} and 1530 cm^{-1}, respectively. This illustrated a typical random coil conformation and amorphous aggregated structure. After gelation of SF with isopropylacrylamide, the characteristic absorption bands of amide I and amide II were identified at 1640 and 1527 cm^{-1}. This indicated that there is a significant conformational transition from random coil to β-sheet during the gelation of SF.[59] The SEM images illustrated the internal structure of the hydrogel (Fig. 1(F)), wherein the porous structure of the hydrogel is clearly observed which may serve as a drug-carrying container. After loading of MTX/ME, the pores of the hydrogel were filled (Fig. 1(G)).

3.2 The dissolution and stabilization of MTX in the IL-ME and the viscoelasticity of the hydrogels

The dissolution capability of MTX was evaluated in PBS (10 mM, pH 7.4), IL-ME and various conventional pharmaceutical solvents, *e.g.*, DMSO, DMF, PEG, IPM, BzH and EA. The solubility of MTX in PBS (10 mM, pH 7.4), DMSO and DMF is 1.75, 0.59 and 0.56 mg mL^{-1}, respectively (Fig. 2(A)), while MTX hardly dissolves in IPM, EA, Ph and PEG (Fig. S4, ESI†). On the other hand, the solubility of MTX in the IL-ME is as high as 17.5 mg mL^{-1}, which can greatly improve the drug availability. The storage of the drug may be closely related to the stability of the solvent. In the present study, the stability of the IL-ME was assessed by observing the size variations of the micellar particles. As shown in Fig. 2(B), the size of micellar particles for the IL-ME remained virtually unchanged after 35 days with respect to that of the fresh IL-ME. The stability of the drug in different solvents was further evaluated. Fig. S3 (ESI†) illustrates that after 30 days a flocculent precipitate was observed in the MTX/PBS system, indicating that MTX is unstable in PBS (10 mM, pH 7.4). As a comparison, however, the MTX/ME micellar system remained clear and transparent under identical experimental conditions. In addition, Fig. 2(C) illustrates that the variation of temperature at 4 °C, 25 °C and 37 °C led to no obvious change in the size of micellar particles. This observation clearly demonstrated that the IL-ME can not only improve the dissolution of the drug, but also serve as a solvent to stabilize the drug.

The hydrogel as a drug carrier should possess favorable adhesion and mechanical properties when it directly comes into contact with human skin. Fig. 2(D) illustrates that the hydrogel could be tightly adsorbed on the skin and would not fall off during joint movement. The adhesion between the hydrogel and the skin is up to 0.015 N, which may readily hold a 3 mL glass vial. It was obvious that the stretched length of the Gel can reach 5 times the original length, illustrating favorable stretchability of the Gel. In tensile tests, the elongation at break of the Gel was increased by 4.1 times, and the tensile strength and maximum tensile force were was enhanced by 5.6 and 5.8 times, respectively, with respect to that of pure PNIPAM hydrogels (Table S1, ESI†). The spreadability study illustrated an obvious increase in the spread diameter of the gel with the increase of SF concentration (Fig. S4A, ESI†). This may be attributed to hydrogen bonding between silk fibroin and isopropylacrylamide.

The swelling behavior of the Gel in the IL-ME or PBS (10 nM, pH 7.4) was evaluated as shown in Fig. S4B (ESI†). The swelling of the Gel in different solvents has the same trend and equilibrium was reached at swelling ratios of 635% and 660%, respectively. This indicates a large drug carrying capacity for the gel. Water loss exclusively depends on the ability of the formulation to form an occlusive layer on the skin. There was almost 5 times more water loss through the filter paper at 48 h

for fluocinonide cream with respect to the ME@Gel (Fig. S5, ESI†). The skin occlusivity offered by the ME@Gel would be helpful for mitigating symptoms like itching, dryness and scaling, which are the main symptoms of psoriasis.

3.3 Drug release and skin permeation capability

The drug release and skin permeability of the thermally responsive hydrogel in the IL-ME were investigated. The release and permeation curves of MTX were obtained using the MTX/PBS@Gel and MTX/ME@Gel at various temperatures, with each formulation containing 1 mg mL^{-1} MTX. The results showed that drug release reached a plateau in 2 h. The release rate of the hydrogel was nearly doubled at 37 °C with respect to that at 25 °C (Fig. 3(A)). This is because the hydrogel transformed from a hydrophilic state to a hydrophobic state at a temperature above LCST (32 °C). This process caused shrinking of the hydrogel network, and thus allowed the drug to be expelled from the gel. At the same temperature, the hydrogel loading MTX/PBS has a higher drug release rate than the hydrogel system with the IL-ME as the drug solvent. The diffusion rate of the MTX/ME@Gel is weakened, possibly due to the high viscosity of the IL-ME. In addition, there are hydrogen bonds between the IL-ME and the Gel. This led to a reduction of the drug release rate and released amount. The permeation-enhancing effects of the IL-ME were evaluated using pig skin. As shown in Fig. 3(B), the drug permeability of the MTX/ME@Gel reached a plateau (32%) at 16 h, while that for the MTX/PBS@Gel is only 5.1%. This indicated a 6-fold increase of drug penetration by the IL-ME.

The mechanism for the enhancement in permeation was investigated using FT-IR spectroscopy. The pig skin was immersed in PBS (10 mM, pH 7.4) or IL-ME of different concentrations at 37 °C for 48 h. To avoid drug interference, the MTX-free IL-ME was used herein. FT-IR spectra showed

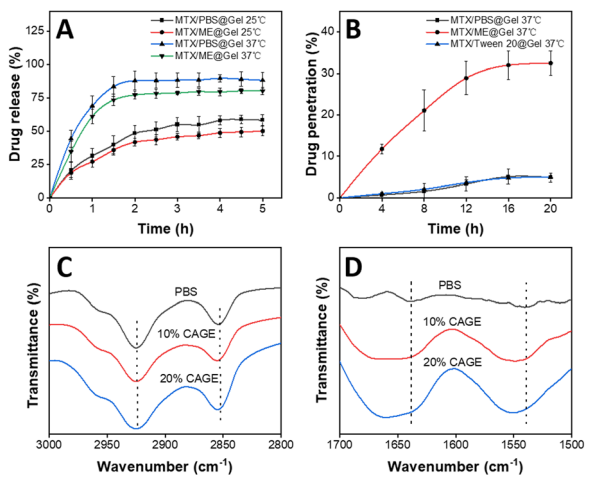

Fig. 3 (A) MTX release profiles of the MTX/PBS@Gel and MTX/ME@Gel at different temperatures. (B) The cumulative percentage of MTX permeation into the pig skin after incubating with the MTX/PBS@Gel MTX/ME@Gel and MTX/Tween 20@Gel for 20 h at 37 °C. FT-IR spectra of pig skin lipids (C) and keratin (D) after treatment with MTX/PBS and MTX/ME (37 °C, 24 h).

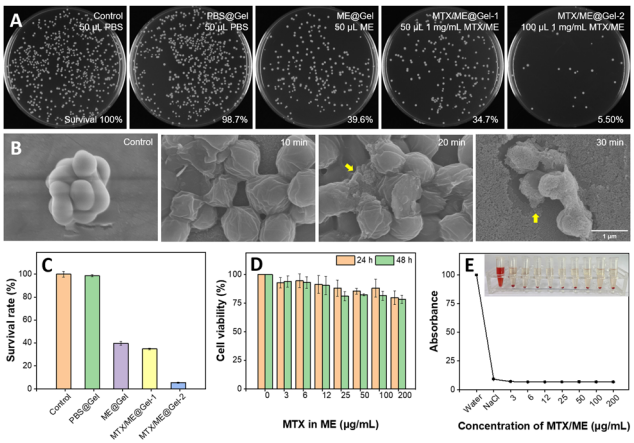

Fig. 4 (A) Representative photographs of microbial colony-forming units (CFUs) after incubation of *S. aureus* for 30 min with PBS (10 mM, pH 7.4), PBS@Gel (50 μL), ME@Gel (50 μL), MTX/ME@Gel-1 (1 mg mL^{-1} MTX, 50 μL of MTX/ME) and MTX/ME@Gel-2 (1 mg mL^{-1} MTX, 100 μL of MTX/ME). (B) SEM images of bacteria (*S. aureus*) after incubation with the MTX/ME@Gel (1 mg mL^{-1} MTX, 100 μL of MTX/ME) for 0, 10, 20 and 30 min. (C) Survival rate of *S. aureus* after incubation with PBS (10 mM, pH 7.4), PBS@Gel (50 μL), ME@Gel (50 μL), MTX/ME@Gel-1 (1 mg mL^{-1} MTX, 50 μL of MTX/ME) and MTX/ME@Gel-2 (1 mg mL^{-1} MTX, 100 μL of MTX/ME) for 30 min. (D) Cell viability of L-02 incubated for 24 h and 48 h in MTX/ME with various concentrations of MTX. (E) Hemolytic activity of various concentrations of MTX in MTX/ME.

changes in the absorption bands associated with lipids and keratin (Fig. 4(C) and (D)). The more the IL in the IL-ME, the greater the change in the absorption band. For IL-ME treated pig skin with 20% CAGE, the C–H vibration bands shifted from 2925 cm^{-1} (asymmetric vibration) to 2927 cm^{-1} and from 2854 cm^{-1} (symmetric vibration) to 2856 cm^{-1}. The vibration bands of NH–C═O shifted from 1639 cm^{-1} to 1643 cm^{-1}, and from 1538 cm^{-1} to 1550 cm^{-1}. These changes may be due to the fact that the IL altered the stratum corneum structure and disrupted the skin's barrier function. The skin lipids are replaced with IL and water, which accelerate drug diffusion.[27]

3.4 *In vitro* antibacterial activity and cytotoxicity assessment

S. aureus was incubated with PBS (10 mM, pH 7.4), Gel, ME@Gel, MTX/ME@Gel-1 and MTX/ME@Gel-2, respectively, for 30 min. It was observed that the pure Gel exhibited very limited or virtually no bactericidal effect (Fig. 4(A)). Meanwhile, the number of colonies in the ME@Gel group was found to show a decrease of *ca.* 60% with respect to that in the control group. MTX/ME@Gel-2 showed significant enhancement in the antibacterial effect with a decrease of the colony number of *ca.* 95.6%. This demonstrated obvious antibacterial activity of the MTX/ME@Gel originating mainly from the IL-ME. SEM images showed obvious shrinking of the bacteria surface after treatment with the MTX/ME@Gel. It was found that the antibacterial activity of the IL-ME was positively correlated with the dose and incubation time (Fig. S6A, ESI†). 0.1 mg mL^{-1} MTX in the MTX/ME@Gel can kill >90% of *S. aureus* in 30 min (Fig. S6B and C, ESI†). The same anti-bacterial activity was observed for *E. coli* (Fig. S7, ESI†). The minimum inhibitory concentration

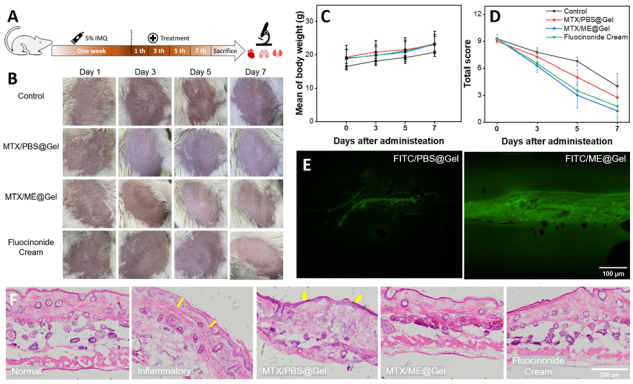

Fig. 5 (A) Schematic representation of modeling and treatment of psoriasis in mice. (B) Photographs of skin on the 1st, 3rd, 5th, and 7th day of treatment (PBS, MTX/PBS@Gel, MTX/ME@Gel, fluocinolone acetate cream). (C) Changes in the body weight of mice on the 1st, 3rd, 5th, and 7th day of treatment. (D) Clinical symptom scores of mouse skin on the 1st, 3rd, 5th, and 7th day of treatment. (E) Fluorescence images after treatment with the FITC/PBS@Gel and FITC/ME@Gel. (F) H&E-stained sections of mouse skin after treatment with PBS, IMQ, MTX/PBS@Gel, MTX/ME@Gel or fluocinolone acetate cream.

was as low as 3 μg mL^{-1} (Fig. S8, ESI†). Cytoplasmic leakage (yellow arrows in Fig. 4(B)) was encountered with increasing treatment time. The result of HO/PI staining indicated the decrease of the number of viable bacteria (blue line), and the increase of the number of dead bacteria (red line) after incubation with the MTX/ME (Fig. S9, ESI†). This further demonstrated the antibacterial activity of the IL-ME.

In addition to the antibacterial capability, the toxicity and side effects of drug carriers are among the focusing issues of the study. The biocompatibility of the MTX/ME@Gel was evaluated by cytotoxicity and hemolysis experiments. After incubating L-02 cells (human normal hepatocytes) in the gel loaded with various amounts of MTX/ME, the cell viability was measured using MTT. Fig. 4(D) indicates cell viabilities of 88% and 81% after 24 h and 48 h incubation with 100 μL MTX/ME (100 μg mL^{-1} MTX). In addition, the red blood cells were collected by centrifugation and further incubated with the MTX/ME (1 mg mL^{-1} MTX) to observe the hemolytic activity. Fig. 4(E) illustrates no obvious hemolysis within the concentration range of 3 to 200 μg mL^{-1} MTX in the IL-ME. This observation indicated favorable biocompatibility of the ME@Gel, which provided a promising candidate as a drug carrier.

3.5 *In vivo* therapeutic study and histopathology

The above discussions based on *in vitro* studies illustrated good skin permeation capability, favorable antibacterial activity and promising biocompatibility for the MTX/ME@Gel. The treatment of mice with the MTX/ME@Gel and the corresponding effects were further investigated, using the experimental process illustrated in Fig. 5(A). A psoriasis mouse model was established by applying 5% imiquimod cream for one week. Fig. 5(B) illustrates that macroscopic fold, redness, scaling, and thickening of the epidermis were clearly observed on the surface of the inflamed skin. The treatment was performed thereafter on the 3rd, 5th and 7th days, and the skin conditions and the change of the body weight of the mice were recorded. The results showed that the redness and swelling of the MTX/PBS@Gel-treated skin were significantly reduced, while the scale was only slightly changed. On treatment with the MTX/ME@Gel, the skin surface showed obviously alleviated redness and decrease of the scaling, the skin surface became smooth and the skin tone was normal. This is essentially the same therapeutic effect as the commercial drug fluocinolone acetate cream. Fig. 5(C) indicates that during the treatment period, the body weight of the four groups of mice increased evenly and rapidly. The clinical symptom score of the Psoriasis Area and Severity Index (PASI) was used to evaluate the severity of skin inflammation. The results illustrated that the thickness, scaling and erythema of the skin for the four groups of mice were treated well (Fig. 5(D) and Fig. S10A, ESI†). The order of the PASI score is MTX/ME@Gel > fluocinolone acetate cream > MTX/PBS@Gel > PBS. This result indicated that the MTX/ME@Gel exhibits excellent therapeutic effects *in vivo*.

The mice were sacrificed after 7 days of the treatment, and the viscera and skin were removed for histopathological evaluation. The results of hematoxylin eosin (H&E) staining indicated that the spleen of the mice in the control group and the MTX/PBS@Gel group exhibited cell proliferation (Fig. S10B, ESI†). The weight of the spleen of the mice of the control group was 4-fold that of the normal mice (Fig. S11, ESI†). This may be caused by the long-term inflammation. In addition, the other visceral weights, and H&E-stained sections of the four groups of mice showed no obvious abnormality. In the IL-ME loaded gel, MTX was replaced by FITC to observe the penetration effect of the gel. The results showed that for the FITC/PBS@Gel group, fluorescence was only recorded on the skin surface of mice. However, the FITC/ME@Gel could readily penetrate the skin through the stratum corneum wherein the fluorescence of FITC was clearly recorded (Fig. 5(E)). H&E-stained sections of the skin at the site of inflammation showed that the inflammatory mice developed stratum corneum thickening, epidermal damage, and cell proliferation (as indicated by the yellow arrow) (Fig. 5(F)). In the MTX/ME@Gel group, these symptoms were significantly alleviated, which was consistent with that treated with fluocinolone acetate cream. The present study indicated that the MTX/ME@Gel can effectively treat psoriasis induced by imiquimod without side effects.

4. Conclusions

A thermo-responsive hydrogel (Gel) loaded with an ionic liquid microemulsion (IL-ME) was demonstrated to be a superb carrier of methotrexate (MTX). The hydrogel incorporating MTX, termed MTX/ME@Gel, provided a promising system for the transdermal delivery of MTX. The hydrogel has good adhesion and mechanical properties. In comparison with the pure PNIPAM hydrogel, the tensile strength of the Gel doped with silk fibroin increased by a factor of 5.6. The IL-ME significantly

increased the solubility of MTX up to 9-fold. As one of the key issues in the transdermal delivery of MTX, the penetration capability of the MTX/ME@Gel was improved up to 6-fold. In addition, the IL-ME provided excellent antibacterial activity for the MTX/ME@Gel. 100 μg mL^{-1} MTX in the MTX/ME@Gel can kill more than 90% of *S. aureus* or *E. coli* in 30 min. *In vivo* experiments further demonstrated that the MTX/ME@Gel can effectively treat IMQ-induced skin inflammation without side effects. Overall, the present study provided a promising approach for the development of a new drug carrier system for improving transdermal delivery capability and enhancing the therapeutic efficiency.

Conflicts of interest

The authors declare that they have no known competing financial interests or personal relationships that could have appeared to influence the work reported in this paper.

Acknowledgements

This work is financially supported by the National Natural Science Foundation of China (No. 21974018, 22174013, and 22074011).

Notes and references

1 R. Parisi, I. Y. K. Iskandar, E. Kontopantelis, M. Augustin, C. E. M. Griffiths and D. M. Ashcroft, *BMJ*, 2020, **369**, m1590.
2 M. Walunj, S. Doppalapudi, U. Bulbake and W. Khan, *J. Liposome Res.*, 2020, **30**, 68–79.
3 M. A. Lowes, C. B. Russell, D. A. Martin, J. E. Towne and J. G. Krueger, *Trends Immunol.*, 2013, **34**, 174–181.
4 Y. Hou, L. Zhu, H. Tian, H. Sun, R. Wang, L. Zhang and Y. Zhao, *Protein Cell*, 2018, **9**, 1027–1038.
5 H. Wang, T. Peters, D. Kess, A. Sindrilaru, T. Oreshkova, N. Van Rooijen, A. Stratis, A. C. Renkl, C. Sunderkötter, M. Wlaschek, I. Haase and K. S. Kochanek, *J. Clin. Invest.*, 2006, **116**, 2105–2114.
6 R. Greenberg, *Cutis*, 2016, **97**, 55–56.
7 E. S. L. Chan and B. N. Cronstein, *Nat. Rev. Rheumatol.*, 2010, **6**, 175–178.
8 A. S. Raut, R. H. Prabhu and V. B. Patravale, *Crit. Rev. Ther. Drug Carrier Syst.*, 2013, **30**, 183–216.
9 D. Aickara, A. M. Bashyam, R. O. Pichardo and S. R. Feldman, *J. Dermatol. Treat.*, 2022, **33**, 512–517.
10 N. Kaur, K. Sharma and N. Bedi, *Pharm. Nanotechnol.*, 2018, **6**, 133–143.
11 L. Sun, Z. Liu, L. Wang, D. Cun, H. Tong, R. Yan, X. Chen, R. Wang and Y. Zheng, *J. Controlled Release*, 2017, **254**, 44–54.
12 M. Qindeel, D. Khan, N. Ahmed, S. Khan and A. Ur Rehman, *ACS Nano*, 2020, **14**, 4662–4681.
13 M. Moniruzzaman, N. Kamiya and M. Goto, *J. Colloid Interface Sci.*, 2010, **352**, 136–142.
14 Y. Poh, S. Ng and K. Ho, *J. Mol. Liq.*, 2019, **273**, 339–345.
15 K. B. Ita, *J. Drug Delivery Sci. Technol.*, 2014, **24**, 245–250.
16 B. Lu, Y. Bo, M. Yi, Z. Wang, J. Zhang, Z. Zhu, Y. Zhao and J. Zhang, *Adv. Funct. Mater.*, 2021, **31**, 2102794–2102806.
17 Y. Hao, W. Zhang, Y. Gao, Y. Wei, Y. Shu and J. Wang, *J. Mater. Chem. B*, 2021, **9**, 250–266.
18 J. Malakar, S. O. Sen, A. K. Nayak and K. K. Sen, *ISRN Pharm.*, 2011, **2011**, 780150.
19 J. Yu, Y. Zhang, Y. Ye, R. DiSanto, W. Sun, D. Ranson, F. S. Ligler, J. B. Buse and Z. Gu, *Proc. Natl. Acad. Sci. U. S. A.*, 2015, **112**, 8260–8265.
20 H. Chen, H. Zhu, J. Zheng, D. Mou, J. Wan, J. Zhang, T. Shi, Y. Zhao, H. Xu and X. Yang, *J. Controlled Release*, 2009, **139**, 63–72.
21 Y. Zhao, M. Moddaresi, S. A. Jones and M. B. Brown, *Eur. J. Pharm. Biopharm.*, 2009, **72**, 521–528.
22 Y. Zhao, S. A. Jones and M. B. Brown, *J. Pharm. Pharmacol.*, 2010, **62**, 678–684.
23 Y. Zhao, M. B. Brown and S. A. Jones, *Nanomedicine*, 2010, **6**, 227–236.
24 M. Hejazifar, O. Lanaridi and K. Bica-Schröder, *J. Mol. Liq.*, 2020, **303**, 112264–112286.
25 D. Dobler, T. Schmidts, I. Klingenhofer and F. Runkel, *Int. J. Pharm.*, 2013, **441**, 620–627.
26 J. Kuchlyan, N. Kundu and N. sarkar, *Curr. Opin. Colloid Interface Sci.*, 2016, **25**, 27–38.
27 C. B. Siqueira Leite, J. M. Coelho, L. A. Muehlmann, R. B. Azevedo and M. H. Sousa, *Curr. Nanosci.*, 2018, **14**, 170–178.
28 Q. M. Qi and S. Mitragotri, *J. Controlled Release*, 2019, **130**, 1873.
29 A. Mandal, N. Kumbhojkar, C. Reilly, V. Dharamdasani, A. Ukidve, D. E. Ingber and S. Mitragotri, *Sci. Adv.*, 2020, **6**, eabb6049.
30 M. Zakrewsky and S. Mitragotri, *J. Controlled Release*, 2016, **242**, 80–88.
31 A. Banerjee, K. Ibsen, Y. Iwao, M. Zakrewsky and S. Mitragotri, *Adv. Healthcare Mater.*, 2017, **6**, 1601411.
32 A. Banerjee, J. Lee and S. Mitragotri, *Bioeng. Transl. Med.*, 2016, **1**, 338–346.
33 A. Banerjee, K. Ibsen, T. Brown, R. Chen, C. Agatemor and S. Mitragotri, *Proc. Natl. Acad. Sci. U. S. A.*, 2018, **115**, 7296–7301.
34 V. Dharamdasani, A. Mandal, Q. M. Qi, I. Suzuki, M. Bentley and S. Mitragotri, *J. Controlled Release*, 2020, **323**, 475–482.
35 T. Hattori, H. Tagawa, M. Inai, T. Kan, S. I. Kimura, S. Itai, S. Mitragotri and Y. Iwao, *Sci. Rep.*, 2019, **9**, 20191.
36 P. Karande, A. Jain, K. Ergun, V. Kispersky and S. Mitragotri, *Proc. Natl. Acad. Sci. U. S. A.*, 2005, **102**, 4688–4693.
37 J. Ko, A. Mandal, S. Dhawan, M. Shevachman, S. Mitragotri and N. Joshi, *Bioeng. Transl. Med.*, 2021, **6**, e10191.
38 E. E. L. Tanner, K. N. Ibsen and S. Mitragotri, *J. Controlled Release*, 2018, **286**, 137–144.
39 S. Uddin, M. R. Islam, M. R. Chowdhury, R. Wakabayashi, N. Kamiya, M. Moniruzzaman and M. Goto, *ACS Appl. Bio. Mater.*, 2021, **4**, 6256–6267.

40 N. Adawiyah, M. Moniruzzaman, S. Hawatulaila and M. Goto, *MedChemComm*, 2016, **7**, 1881–1897.
41 M. K. Ali, R. M. Moshikur, R. Wakabayashi, M. Moniruzzaman, N. Kamiya and M. Goto, *ACS Sustainable Chem. Eng.*, 2020, **8**, 6263–6272.
42 M. R. Chowdhury, R. M. Moshikur, R. Wakabayashi, Y. Tahara, N. Kamiya, M. Moniruzzaman and M. Goto, *Mol. Pharmaceutics*, 2018, **15**, 2484–2488.
43 M. R. Islam, M. R. Chowdhury, R. Wakabayashi, N. Kamiya, M. Moniruzzaman and M. Goto, *Pharmaceutics*, 2020, **12**, 392.
44 M. R. Islam, M. R. Chowdhury, R. Wakabayashi, Y. Tahara, N. Kamiya, M. Moniruzzaman and M. Goto, *Int. J. Pharm.*, 2020, **582**, 119335.
45 R. M. Moshikur, M. R. Chowdhury, H. Fujisawa, R. Wakabayashi, M. Moniruzzaman and M. Goto, *ACS Sustainable Chem. Eng.*, 2020, **8**, 13660–13671.
46 S. Uddin, M. R. Chowdhury, R. Wakabayashi, N. Kamiya, M. Moniruzzaman and M. Goto, *Chem. Commun.*, 2020, **56**, 13756–13759.
47 R. M. Moshikur, M. R. Chowdhury, R. Wakabayashi, Y. Tahara, M. Moniruzzaman and M. Goto, *Int. J. Pharm.*, 2018, **546**, 31–38.
48 J. Li and D. J. Mooney, *Nat. Rev. Mater.*, 2016, **1**, 16071.
49 S. Bernhard and M. W. Tibbitt, *Adv. Drug Delivery Rev.*, 2021, **171**, 240–256.
50 L. A. Lyon, Z. Meng, N. Singh, C. D. Sorrell and A. John, *Chem. Soc. Rev.*, 2009, **38**, 865–874.
51 Z. Han, P. Wang, G. Mao, T. Yin, D. Zhong, B. Yiming, X. Hu, Z. Jia, G. Nian, S. Qu and W. Yang, *ACS Appl. Mater. Interfaces*, 2020, **12**, 12010–12017.
52 J. Nan, Y. Chen, R. Li, J. Wang, M. Liu, C. Wang and F. Chu, *Nano-Micro Lett.*, 2014, **6**, 200–208.
53 J. Park, S. Pramanick, D. Park, J. Yeo, J. Lee, H. Lee and W. J. Kim, *Adv. Mater.*, 2017, **29**, 1702859.
54 L. Tang, L. Wang, X. Yang, Y. Feng, Y. Li and W. Feng, *Prog. Mater. Sci.*, 2021, **115**, 100702.
55 M. A. Haq, Y. Su and D. Wang, *Mater. Sci. Eng., C*, 2017, **70**, 842–855.
56 M. Farokhi, F. Mottaghitalab, Y. Fatahi, A. Khademhosseini and D. L. Kaplan, *Trends Biotechnol.*, 2018, **36**, 907–922.
57 Y. Gao, Y. Hao, W. Zhang, Y. Wei, Y. Shu and J. Wang, *Chem. Eng. J.*, 2022, **429**, 131590.
58 M. K. Ali, R. M. Moshikur, R. Wakabayashi, M. Moniruzzaman and M. Goto, *ACS Appl. Mater. Interfaces*, 2021, **13**, 19745–19755.
59 S. Chen, S. Liu, L. Zhang, Q. Han, H. Liu, J. Shen, G. Li, L. Zhang and Y. Yang, *Chem. Eng. J.*, 2020, **399**, 125795.

